Journal of Marine Science and Application (2026) 25: 95-109
https://doi.org/10.1007/s11804-025-00684-7

RESEARCH ARTICLE

Effect of Spudcan Penetration Angles on Adjacent Bucket Foundation in Sand

Conghuan Le[1], Zhenqi He[1], Hao Hu[1], Puyang Zhang[1] and Hongyan Ding[1]

Received: 10 October 2024 / Accepted: 30 December 2024

Abstract

Installing internal bulkheads in a composite bucket foundation alters the rotational symmetry characteristic of a single-compartment bucket foundation, consequently influencing the stress distribution within the bucket and surrounding soil. During the seabed penetration of a spudcan from a jack-up wind turbine installation vessel, an angle may form between the spudcan's axis and the axis of symmetry of the adjacent composite bucket foundation in the horizontal plane. Such a misalignment may affect load distribution and the non-uniform interaction between the foundation, soil, and spudcan, ultimately influencing the foundation's stability. This study employs physical model tests to ascertain the trends in end resistance during spudcan penetration in sand, the extent of soil disturbance, and the backflow condition. The finite element coupled Eulerian–Lagrangian method is validated and utilized to determine the range of penetration angles that induce alterations in the maximum vertical displacement and tilt rate of the composite bucket foundation in sand. The differential contact stress distribution at the base of the bucket is analyzed, with qualitative criteria for sand backflow provided. Findings demonstrate that the maximum vertical displacement and tilt rate of the composite bucket foundation display a "wave-like" variation with the increasing spudcan penetration angle, peaking when the angle between the spudcan and bulkhead is the smallest. Stress distribution is predominantly concentrated at the base and apex of the bucket, becoming increasingly uneven as the penetration angle deviates from the foundation's symmetry axis. The maximum stress gradually shifts to the junction of the bulkhead and bucket bottom on the side with the shortest net distance from the spudcan. Considering the in-place stability and stress state of the composite bucket foundation is therefore imperative, and particular attention should be paid to the foundation's state when the angle between the spudcan and bulkhead is small.

Keywords Spudcan penetration; Soil disturbance; Penetration angle; Composite bucket foundation; Coupled Eulerian–Lagrangian

1 Introduction

In light of the diminishing reserves of traditional fossil fuels and mounting pressures on the environment, reducing fossil fuel consumption, curbing greenhouse gas emissions, and developing renewable energy have emerged as pivotal trends in global energy advancement. Wind energy represents an important branch of renewable energy, offering a sustainable and non-polluting source of energy that is instrumental in advancing renewable energy solutions (Ma et al., 2025; Zhang et al., 2019). Oceans, with their abundant resources, stable wind conditions, high hours of power generation utilization, absence of land occupation, minimal impact on the ecological environment, lack of water consumption, and suitability for large-scale development, have become key sites for wind power generation (Dao et al., 2020). Given the distinctive and intricate nature of the marine environment (Zhang et al., 2020), the foundation is a critical element in the construction of offshore wind turbines. The composite bucket foundation has gained significant attention in offshore wind power construction due to its efficiency and low cost. Installed using a jack-up wind turbine installation vessel, it has become a common method for deploying fixed-bottom offshore wind turbines. During operation, the jack-up wind turbine installation vessel is supported by its legs on the seabed through spudcan penetration, with the hull raised to ensure operational stability in complex marine environments. However, the operational cantilever length limits the positioning of the operational site, which must be close to the offshore wind turbine platform. The soil squeezing effect generated during spudcan penetration can impose additional loads on adjacent foundations (Siciliano et al., 1990). In severe cases,

Article Highlights

- A scaled spudcan penetration test in sand defines the soil disturbance range and validates the coupled Eulerian–Lagrangian method.
- The effect of spudcan penetration angles on sand backflow, bucket foundation displacement, and stress are studied.
- Finds indicate that attention is needed to the bucket foundation's state when the spudcan penetrates at small angles relative to the bulkhead of the bucket foundation.

✉ Conghuan Le
leconghuan@163.com

[1] State Key Laboratory of Hydraulic Engineering Intelligent Construction and Operation, Tianjin University, Tianjin 300072, China

this effect can lead to instability, excessive deformation, and other adverse effects (Li et al., 2018).

The study of spudcan–soil–adjacent foundation interactions can be categorized into two principal approaches: test research and numerical simulations. Test research can be further subdivided into standard gravity (1 g) tests and centrifuge tests. Standard gravity tests, because of their low stress levels, often exhibit notable discrepancies in soil bearing capacity relative to actual conditions. Therefore, centrifuge tests, which replicate in-situ stress levels, are the preferred methodology (Craig and Chua, 1990). A series of centrifuge tests were conducted to investigate the effect of spudcan penetration on pile bending moments and soil flow around piles of adjacent jacket platforms under conditions of soft clay and sand overlying soft clay. The results indicated that factors such as spudcan penetration depth, pile spacing, pile length, overlying clay thickness, and penetration time influence the bending moments of adjacent jacket platform piles. Specifically, the bending moment increases with penetration depth and decreases with pile spacing. In contrast, longer piles and thicker clay layers help mitigate the pile bending moment (Xie, 2009; Xie et al., 2012; Xie et al., 2017). The effect of spudcan penetration on the bending moment distribution of adjacent single pile foundations in uniform clay and clay with an overlying sand layer was investigated through standard gravity (1 g) tests. The results showed that the bending moment induced by spudcan penetration is greater in clay with an overlying sand layer than in uniform clay (Falcon et al., 2021). The influence range of spudcan penetration and extraction in sand, along with the corresponding changes in soil strength, was studied through a combination of model tests and theoretical analysis. A theoretical method was proposed for calculating the bearing capacity of the adjacent spudcan within the affected zone. The study found that when the relative distance between two spudcans exceeds twice the diameter of the penetrating spudcan, the penetration and extraction do not affect the bearing capacity of the adjacent spudcan foundation (Liu et al., 2020).

The complexity of factors affecting soil mechanical properties presents a major challenge to studying large deformation phenomena resulting from spudcan–soil interactions using analytical methods and traditional numerical approaches (Bui et al., 2008; Qiu et al., 2011). To address this issue, more effective numerical simulation methods have been adopted (Wang et al., 2015; Chouhan and Chavda, 2021). Qiu et al. employed the coupled Eulerian–Lagrangian (CEL) method in ABAQUS to simulate a range of problems, including strip foundation footings, pile penetration, and ship grounding. A comparison of finite element method results and field measurements demonstrated the robustness and efficiency of the CEL method. Subsequently, this method was employed in marine geotechnics to investigate the penetration of spudcan foundations of jack-up drilling platforms into the seabed (Qiu and Henke, 2011). The findings align with the existing analytical results and centrifuge test data (Craig and Chua, 1990; Teh et al., 2008). The CEL method was employed to investigate the effects of continuous spudcan penetration on adjacent pile foundations for jack-up drilling platforms (Tho et al., 2013). Their results corresponded with Xie et al.'s centrifuge tests (Xie, 2009), further confirming the feasibility of the method in marine geotechnics. In addition to the CEL method, A novel approach was introduced for calculating the response of an adjacent pile foundation to spudcan penetration. This method employs large deformation finite element analysis to extract variations in pile deflection caused by spudcan penetration and transform them into equivalent nodal loads on a nonlinear beam on an elastic foundation. These additional loads are then determined on the pile. The efficacy of this methodology was substantiated through 50 g centrifuge tests (Fan and Wang, 2021). A simple yet effective "remeshing and interpolation technique with small strain" approach for large deformation finite element (LDFE) analysis in geomechanics was proposed. The robustness and numerical accuracy of this method were validated through four case studies, including the penetration of structures with varying shapes and sizes, plate anchor anchorage, and shallowly buried subsea pipelines (Tian et al., 2014). In addition to pile foundations, researchers focused their attention on wide and shallow bucket foundations. A physical model test and the CEL method were employed to investigate the influence of the ratio between the clear distance from the spudcan to the composite bucket foundation and the spudcan diameter on the in-place stability of an adjacent bucket foundation during spudcan penetration (Le et al., 2024). The effect of spudcan penetration speed on the insertion performance of bucket spudcans in saturated sand was examined through small-scale model tests. Based on foundation bearing capacity theory, a method for calculating penetration resistance was proposed. The penetration process was simulated using CEL finite element analysis and compared with experimental results (Wu et al., 2018).

Despite extensive research on the influence of spudcan penetration on adjacent pile foundations, relatively few studies investigate the effect on bucket foundations, which are widely used in offshore wind power and differ from pile foundations. Unlike the symmetrical configuration of pile foundations, the internal bulkheads of composite bucket foundations influence structural strength and soil partitioning. A discrepancy between the spudcan penetration angle and the foundation's symmetry axis may increase stress unevenness and alter the interactions between the bucket, soil, and spudcan, potentially affecting the in-place stability of the foundation. Accordingly, this study employs physical model tests and the CEL method to investigate the influence of the relative angle between the spudcan and bucket

foundation formed during penetration on the in-place stability and contact stress distribution of the composite bucket foundation.

2 Spudcan penetration test design

The composite bucket foundation is gaining attention in offshore wind power for its efficiency, low cost, and enhanced floating stability, making it ideal for wet tow transportation (Zhang et al., 2013; Zhang et al., 2023) and improving construction efficiency (Hossain and Randolph, 2010; Ding et al., 2019; Ding et al., 2020), as illustrated in Figure 1. With the scaling up of offshore wind power development, efficient construction and operation & maintenance have become key industry priorities. In this context, jack-up wind turbine installation vessels, known for their multifunctional integration, high load-bearing capacity, and stability, are widely used for the transportation, installation, and maintenance of wind turbines, as illustrated in Figure 2 (Shi et al., 2024; Domingos et al., 2024). These vessels maintain stability by using spudcans at their base, which penetrate the seabed to provide strong support, ensuring the vessel remains stable under the effects of waves and currents, thereby facilitating the installation of wind turbines. However, the soil squeezing effect generated during spudcan penetration in sand may affect the in-place stability of the adjacent foundation. Given the high cost of physical model testing, conducting a comprehensive study under all possible design conditions are impractical. This chapter presents the design of a physical model test for spudcan penetration in sand. The objective is to elucidate the trend of penetration resistance with depth, the extent of soil disturbance caused by spudcan penetration, and the soil backflow mechanism at the spudcan site. The results are compared with those obtained using the CEL method to validate the accuracy of the physical model test, thereby supporting further numerical simulation studies under various design conditions.

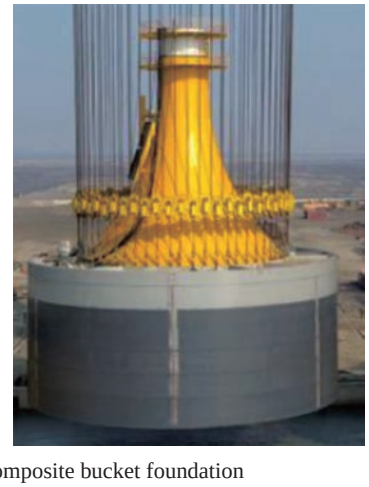

Figure 1 Composite bucket foundation

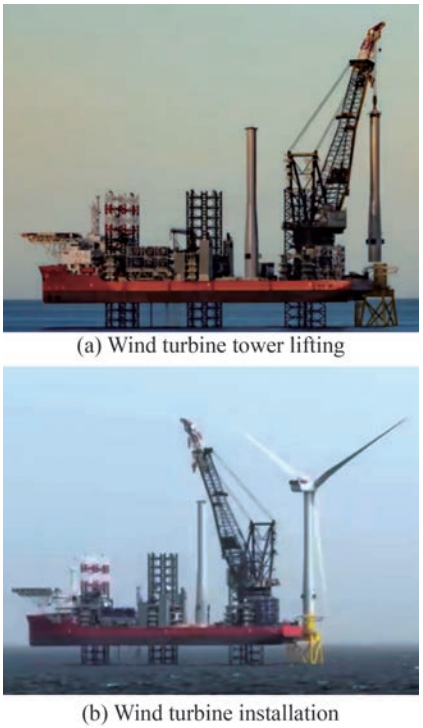

(a) Wind turbine tower lifting

(b) Wind turbine installation

Figure 2 Schematic of a jack-up wind turbine installation vessel

2.1 Test model and instrument layout

The experiments were conducted in a soil container with dimensions of 2 m × 2 m × 1 m. Fujian standard sand was used as the test soil, and its parameters were determined through geotechnical testing, as presented in Table 1. The particle size distribution curve is depicted in Figure 3. A layer of gravel, with particle sizes ranging from 5 to 20 mm, was laid at the bottom of the soil container at a depth of 0.2 m. Drainage pipes were installed over the gravel layer and covered with geotextile fabric. To guarantee uniformity of the soil across different locations, the sand was added using the sand rain method, with the objective of achieving the designed elevation of the soil surface. The layout of the soil container is illustrated in Figure 4. The spudcan model, made of stainless steel, was scaled to 1∶100 in accordance with the engineering design specifications, with the precise dimensions shown in Figure 5.

The test was conducted in accordance with standard gravity conditions, namely, 1 g. The spudcan penetration depth was set to 1.5 times the height of the spudcan, rounded up to a value of 60 mm, following a standardized procedure. The penetration speed was maintained at 3.6 mm/s. To guarantee accurate data collection and analysis, the test setup incorporated a high-power worm gear vertical loading apparatus capable of applying a maximum load of 10 000 N. Load control was achieved by adjusting the voltage to regulate the loading speed. A stainless steel reaction frame was used to support the loading device. The setup also

Table 1 Parameters of Fujian standard sand

Soil properties	Specific gravity	Maximum dry density (g/cm^3)	Minimum dry density (g/cm^3)	Relative density	Elastic modulus (MPa)	Internal friction angle (°)	Permeability coefficient (cm/s)
Standard sand	2.42	1.50	1.28	0.58	18	32.5	0.039

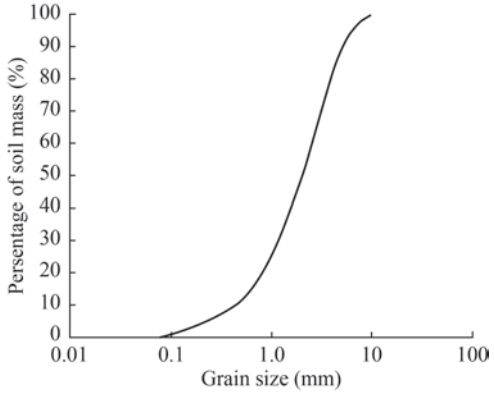

Figure 3 Particle gradation curve of sand

included a Weekend WKD3840 (Tianjin Weekend Measurement and Control Equipment Technology Co., Ltd., Tianjin, China) strain gauge data acquisition system with a sampling frequency of 10 Hz. Additionally, various sensors were utilized, including soil pressure sensors (range: 0 – 50 kPa) for monitoring soil pressure fluctuations and the impact area of the spudcan penetration; laser displacement sensors (range: ±200 mm) for measuring the depth of spudcan penetration; wire displacement sensors (range: 0–500 mm) for cross-checking and correcting measurements from the laser sensors; and load cells (range: 3 000 N) for measuring resistance during spudcan penetration and removal. The specific layout of the test setup is shown in Figure 6.

To accurately observe the dynamic changes in the soil during spudcan penetration into the sand, soil pressure sensors were pre-installed at a depth of 1 cm below the soil surface at distances of 0.5d, 1.0d, 1.5d, 2.0d, and 2.5d from the long edge of the spudcan (where d is the length of the spudcan's long edge). After preparing the test setup, sensors, and soil container, the system was allowed to settle for 12 h to minimize the effects of soil disturbance. Figure 7 illustrates the spudcan penetration.

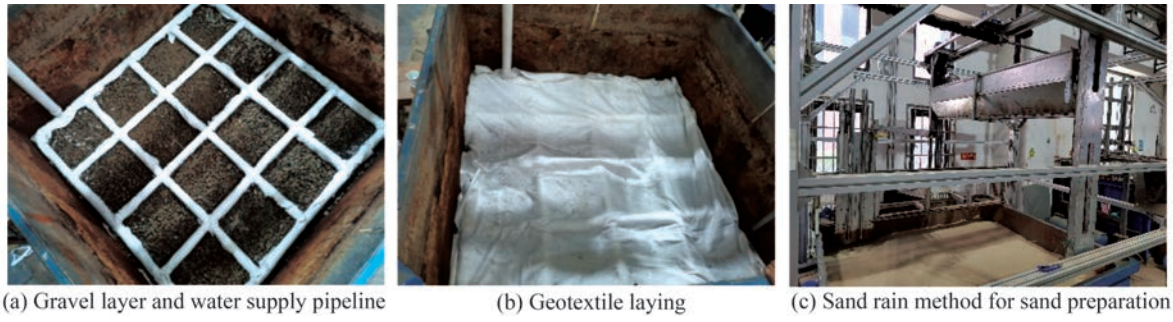

Figure 4 Soil container layout

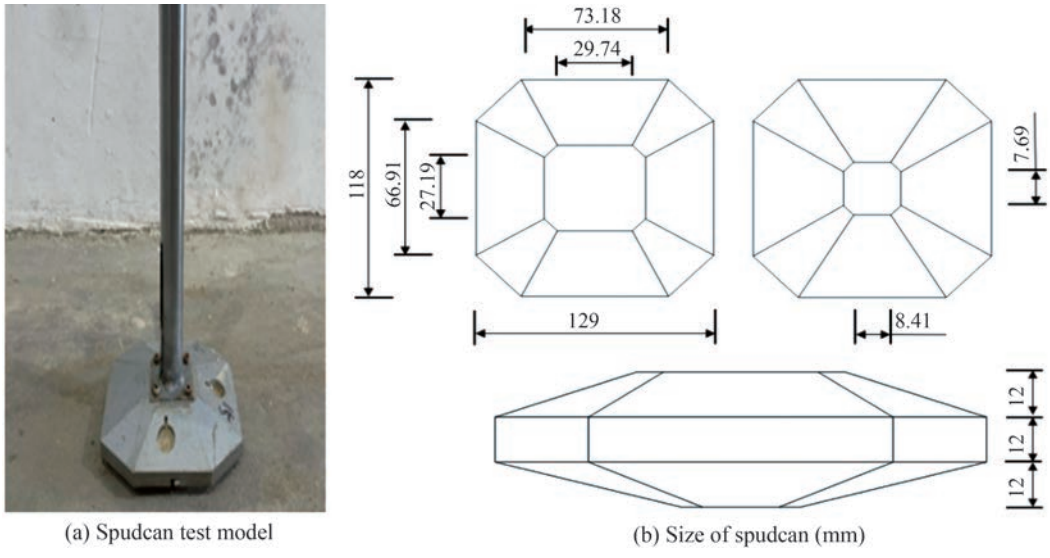

Figure 5 Schematic of spudcan structure

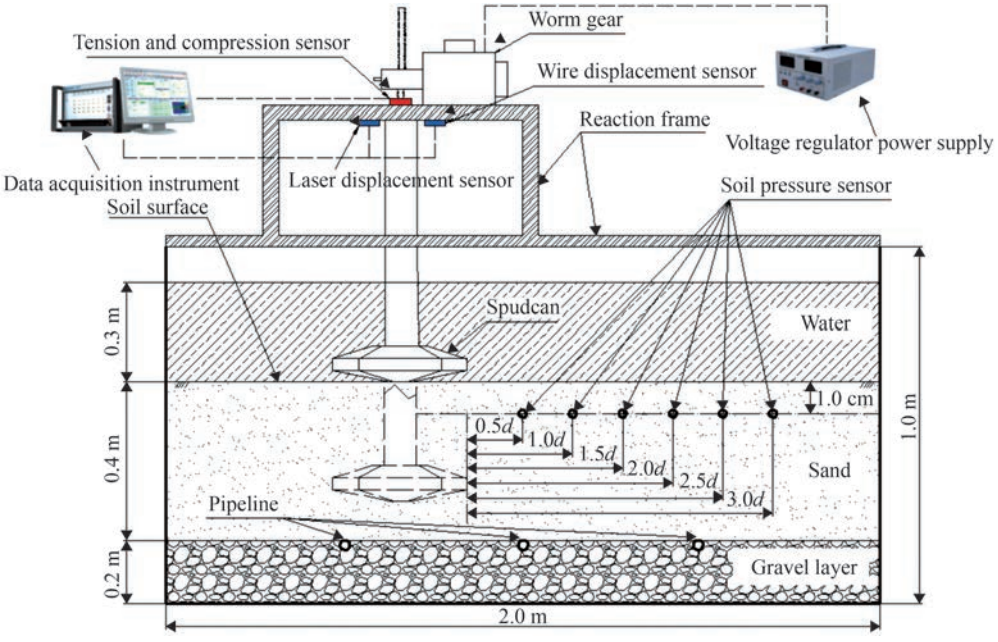

Figure 6 Schematic of test apparatus layout

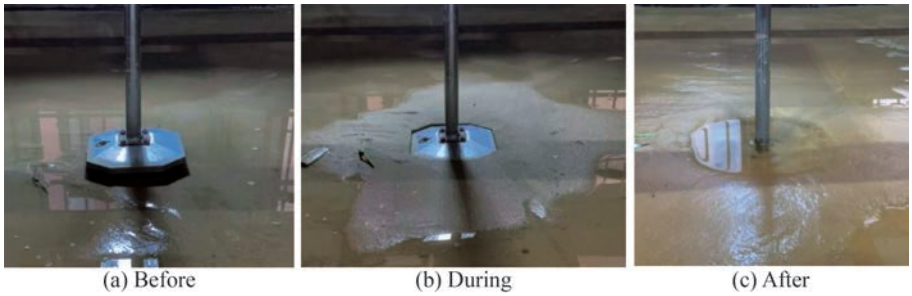

Figure 7 Spudcan penetration

2.2 Comparison between the CEL method and model testing

The soil dimensions, soil parameters and spudcan dimensions in the CEL model were consistent with those observed in the physical model test. The dimensions of the soil model were 2 m × 2 m × 1 m, comprising Eulerian elements with a void layer of 0.4 m. To guarantee computational accuracy and efficiency, the fine mesh size was set to 0.6 mm (approximately 0.05 times the diameter of the spudcan), and the fine mesh region was defined as twice the spudcan diameter (Dai et al., 2018). The boundary conditions included normal constraints in the X and Y directions, full constraints at the bottom of the soil, and a free surface at the top. The spudcan was modeled using steel material, and rigid body constraints were employed to enhance computational efficiency because spudcan deformation was not considered. The specific model is illustrated in Figure 8.

To guarantee a quasistatic penetration while maintaining computational efficiency, the spudcan was required to penetrate at a uniform speed of 0.2 m/s to a depth of 6 cm in sand. Figure 9(a) illustrates the variation in soil pressure at distinct observation points relative to the depth of spudcan penetration, as determined through the physical model test. The soil at the 0.5d position exhibited the most notable backflow in response to the spudcan penetration, resulting in pit refilling and minimal soil pressure fluctuation, with a maximum of 0.5 kPa. The soil pressure at the 1.0d position exhibited the most pronounced variation, initially increasing and then decreasing as penetration depth increased. The maximum soil pressure of 3.55 kPa was reached at a penetration depth of 38.81 mm. The variation in soil pressure at positions 1.5d to 2.5d exhibited a decreasing trend as monitoring distance increased. The overall trend indicated that soil pressure increased with penetration depth. The alterations observed at the 1.5d position were similar to those documented at the 1.0d position, exhibiting a descending trajectory following the inflection point. No significant change in soil pressure was observed at the 2.5d position. Therefore, spudcan penetration causes the greatest disturbance to the soil within the range of 1.0d, gradually decreasing beyond this point. The influence of soil heaving and pressure changes is negligible

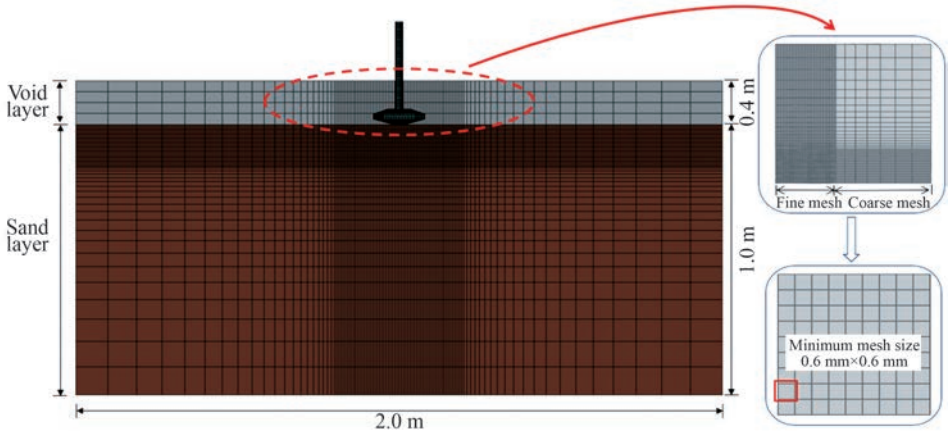

Figure 8 CEL model

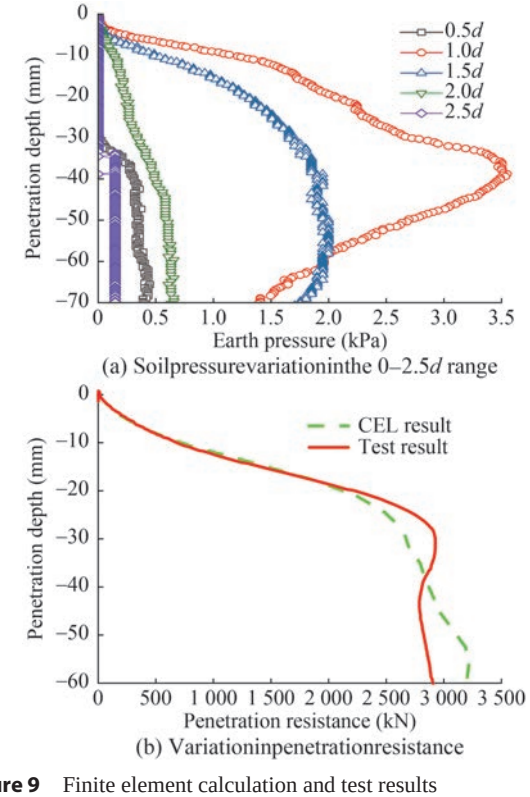

Figure 9 Finite element calculation and test results

beyond a distance of 2.0*d* from the spudcan edge, and the effect is almost undetectable at a distance of 2.5*d*. The range of the soil squeezing effect is consistent with the findings of a previous study (Zhou et al., 2023).

A comparison between the calculated results of the CEL method and the measured penetration depth–resistance curve is presented in Figure 9(b). The figure illustrates that the overall trend of the CEL method results is comparable to that of the physical model test results. Both curves display an inflection point at approximately 30 mm penetration depth. Before the inflection point, the fluctuations in both sets of results are nearly indistinguishable. After the inflection point, the experimental results demonstrate a discernible decline in penetration resistance, followed by a gradual increase. In contrast, the CEL calculation results exhibit a progressive rise in penetration resistance. The maximum discrepancy in penetration resistance between the CEL method and the experimental results near the inflection point is 7.96%, but the difference reaches 10.06% at the final penetration depth. In the CEL finite element simulation, increasing the speed of spudcan penetration from 0.2 to 20 cm/s results in a negligible difference in the insertion resistance curve. This outcome indicates that the dynamic response in the numerical simulation can be disregarded at this stage. Consequently, spudcan penetration can be regarded as a quasi-static process, and the influence of the penetration speed on the penetration resistance is limited. To ensure the quasistatic process, the penetration speed of 3.6 mm/s is employed in the model test, and the penetration speed of the CEL finite element simulation is set to 0.2 m/s. This approach ensures computational efficiency and minimizes the influence of the dynamic response on the penetration resistance caused by excessive penetration speed, making it a feasible method. Figure 10 illustrates the soil flow around the spudcan at the designed depth, as simulated by the CEL method and observed in the model test. The figure demonstrates that the soil flow pattern simulated by the CEL method is similar to that observed in the model test. A slight heaving of the surrounding soil surface is observed after spudcan penetration, accompanied by collapse and backflow of soil at the penetration location. This process results in the formation of a spudcan pit, which subsequently covers the spudcan with backfilled soil. Thus, the CEL method provides an accurate representation of the soil disturbance and backflow state resulting from spudcan penetration.

In conclusion, the CEL method exhibits a consistent variation pattern in the penetration depth–resistance curve during spudcan penetration when compared with the data from the physical model test. The method qualitatively captures the phenomena of soil disturbance and backflow. Therefore, the CEL method is an effective tool for simulating spudcan penetration in sand.

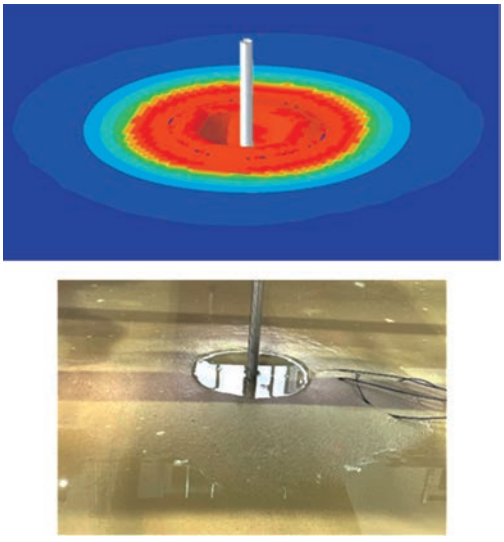

Figure 10 Finite element analysis results compared with test data

3 Effects of spudcan penetration angle on adjacent bucket foundations

3.1 CEL model

The overall CEL calculation model comprises a multi-compartment bucket foundation, an upper transition section, a spudcan, pile legs, and surrounding soil, as illustrated in Figure 11. The multicompartment bucket foundation, spudcan, and pile legs are constructed from steel with a density of 7 850 kg/m³, a modulus of elasticity of 210 GPa, and a yield strength of 355 MPa. These specifications are scaled according to the specific engineering project, as shown in Figure 12. The objective of this study is to examine the effect of spudcan penetration angle on adjacent multi-compartment bucket foundations, so the dimensions D, u, d, H, h, and L remain constant. D represents the diameter of the bucket foundation, equating to 25.6 m. The value of u, which is the edge length of the hexagonal bulkhead situated in the central compartment, is 6.4 m. The length of the spudcan's long edge, d, is 11.8 m. The height of the bucket foundation, H, is 10 m, and the height of the transition section, h, is 28 m. The length of the pile legs, L, is 20 m. In accordance with Section 2.2, the spudcan penetration causes the greatest soil disturbance within a range of 1.0d, with minimal effect beyond 2.0d. In this section, the net distance between the bucket foundation and the spudcan edge is set to S = 1.5, d = 17.7 m for the purpose of calculation. The composite bucket foundation is embedded to a depth of 10 m below the soil surface. To simulate the effect of spudcan penetration-induced soil displacement on the adjacent foundation in a computationally efficient manner, the spudcan penetration depth is set to 10 m, which matches the foundation's burial depth. The use of rigid body constraints enhances computational efficiency because the deformation effects of the foundation and spudcan are not considered. The soil material is sand, which is modeled using Eulerian elements, and a void layer of 10 m is incorporated into the model. The Mohr–Coulomb yield criterion is employed. To guarantee computational accuracy and efficiency, the fine mesh size is set to 0.5 m (approximately 0.05 times the spudcan diameter), and the fine mesh region extends to twice the spudcan diameter (Tho et al., 2013). The soil parameters used in the model are consistent with those observed in the experiment: density ρ = 1 400 kg/m³, internal friction angle Ψ = 32.5°, compression modulus Es = 18 MPa, and Poisson's ratio μ = 0.3. In actual engineering practice, the bucket foundation is often settled until the top surface compresses the soil, thereby creating a transition section that is above the soil surface and not directly affected by the spudcan-induced soil displacement. As such, this effect is excluded from subsequent analyses.

This study employs a six-compartment bucket foundation, as outlined in the Methodology section. In consideration of structural symmetry, the variation in spudcan penetration angle is analyzed within a single compartment, representing half of the total compartmentalized area. The operational conditions are illustrated in Figure 13.

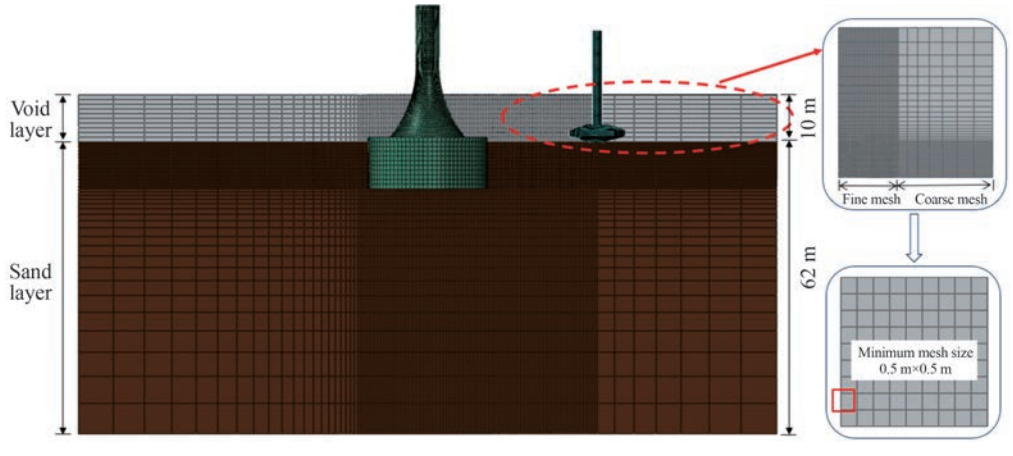

Figure 11 Overall CEL model

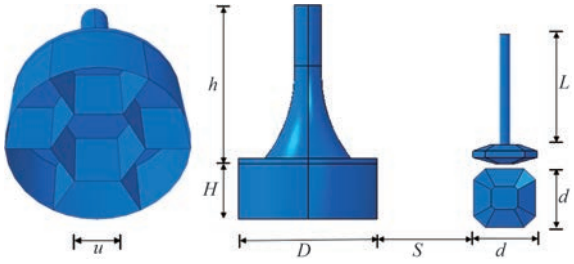

Figure 12 Bucket foundation with spudcan model

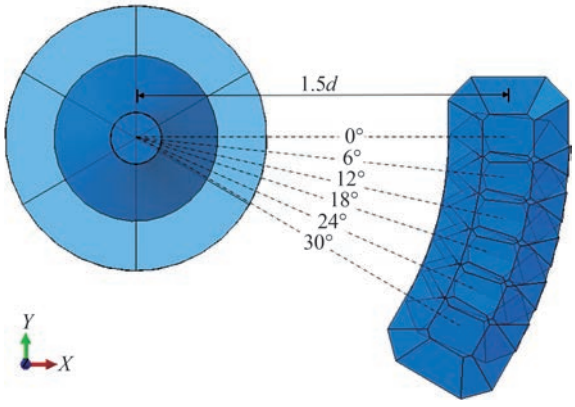

Figure 13 Illustration of different spudcan penetration angles

3.2 Effect of spudcan penetration angle on soil backflow

Figure 14 illustrates the equivalent plastic strain contour maps of the soil surrounding the spudcan at different penetration angles. For each angle, the soil around the spudcan exhibits heaving behavior, but no significant soil backflow is observed within the spudcan pit, indicating that the backflow capacity of the hard sand is limited. The distribution of equivalent plastic strain at the base of the spudcan is concave. As the penetration angle increases, the equivalent plastic strain initially decreases before increasing, reaching its minimum at 12° and maximum at 30°. To elucidate the trend of the maximum equivalent plastic strain during this process, normalization is conducted using the peak value, as illustrated in Figure 15. Considering structural symmetry, the solid line in the figure represents the maximum equivalent plastic strain around the spudcan for different penetration angles, calculated using the CEL method for a half compartment, and the dashed line represents the corresponding scenario for a symmetric half compartment. Moreover, the spudcan penetration angle affects the distribution of equivalent plastic strain in the soil. At a 0° penetration angle, the soil on the side of the spudcan away from the bucket foundation exhibits greater equivalent plastic strain than the side closer to the foundation. Conversely, for other penetration angles, the side closer to the foundation exhibits higher strain. These findings suggest that the interaction between the spudcan and the multi-compartment bucket foundation at different angles exerts a varying influence on the plastic deformation of the soil near the spudcan.

3.3 Effect of spudcan penetration angle on the displacement of bucket foundation

Figure 16 depicts the vertical displacement of the upper surface of the multi-compartment bucket foundation under varying spudcan penetration angles. The *X*-axis represents the line connecting the center of the spudcan and the multi-compartment bucket foundation. As illustrated in the figure, the vertical displacement on the side of the foundation's top surface farthest from the spudcan is consistently greater than on the side closest to the spudcan. Thus, the inclination direction of the foundation corresponds to the penetration direction of the spudcan. As the spudcan penetration angle varies from 0° to 30°, the maximum vertical displacement and tilt rate of the multi-compartment bucket foundation exhibit a wavelike pattern. The maximum vertical displacement differences are relatively small, ranging from approximately −0.018 to −0.016 m, whereas the tilt rate demonstrates significant variation, with values of 0.28‰, 0.42‰, 0.36‰, 0.32‰, 0.45‰, and 0.34‰ for the respective penetration angles. To elucidate the trend of the tilt rate throughout the process, the variation at the symmetrical half-compartment position is depicted, as referenced in Section 3.2 and shown in Figure 17. When the absolute spudcan penetration angle ranges from 0° to 12°, the trends of the maximum vertical displacement and tilt rate are opposite. Beyond this range, the trends become similar. This indicates that the bulkheads have varying effects on the multi-compartment bucket foundation depending on the spudcan penetration angle. Accordingly, a differential impact range can be defined, with the symmetric axis of a compartment representing a penetration angle of 0°, extending approximately ±12° on both sides. Within this range, the trends of vertical displacement and tilt rate are opposite, forming a reverse zone. Beyond this range, up to the compartment boundary, the observed trends are identical, forming a concordant zone.

3.4 Effect of spudcan penetration angle on stress in the bucket foundation

Figure 18 illustrates the stress distribution in the wall of the bucket foundation following spudcan penetration to a depth of 10 m. For varying spudcan penetration angles, the stress is predominantly concentrated near the spudcan, particularly at the top and bottom of the bucket. The stress distribution and magnitude at the bucket bottom are more pronounced than at the top, with a significant concentration of stress occurring at the junction between the bulkhead nearest to the spudcan and the bucket bottom. At a penetration angle of 0°, the maximum contact stress forms a "belt-like" distribution along the junctions of the 30° and 330°

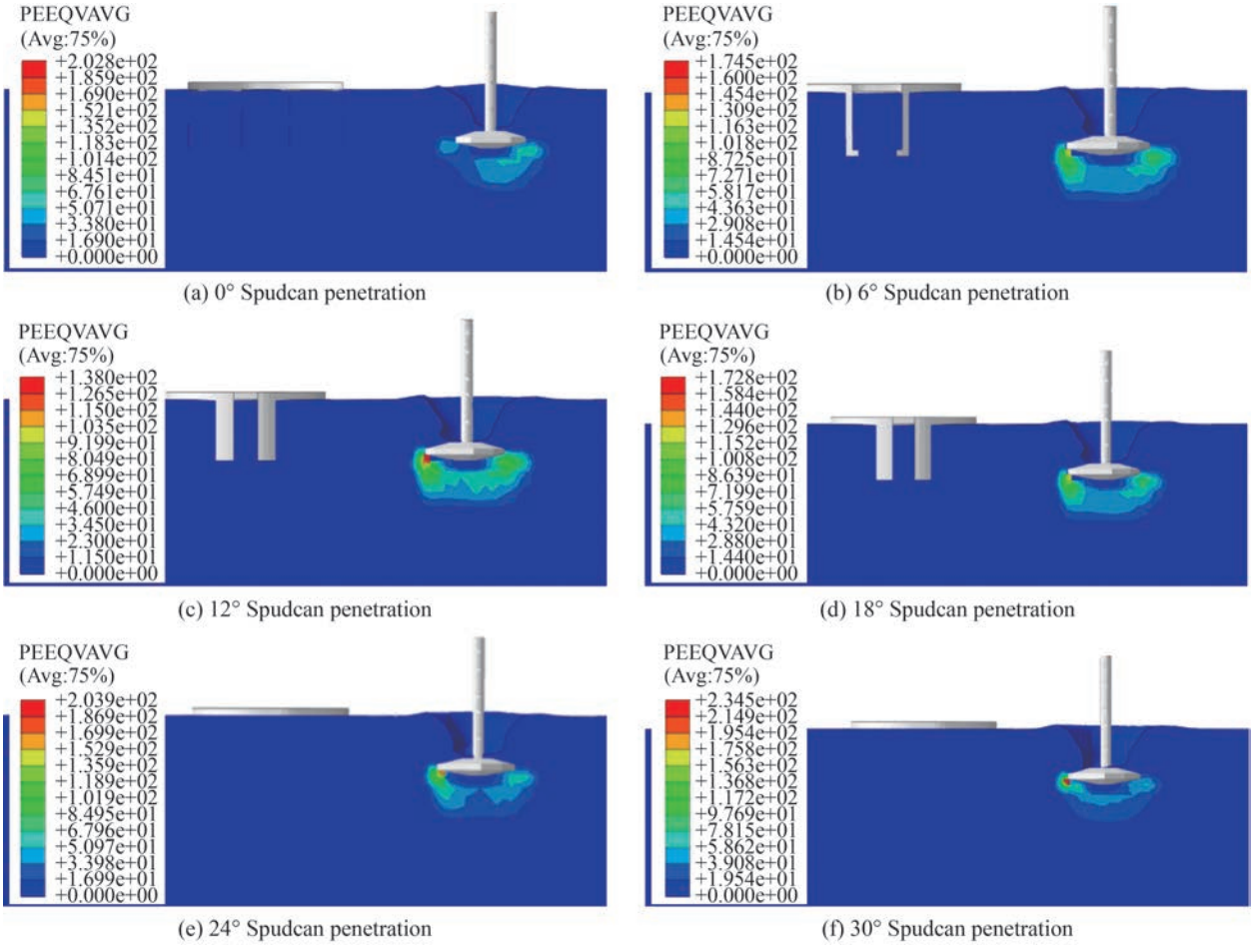

Figure 14 Soil movement around the spudcan at different penetration angles

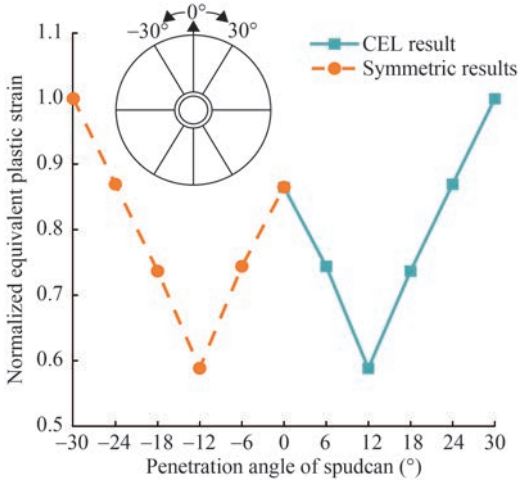

Figure 15 Maximum equivalent plastic strain around the spudcan at different penetration angles

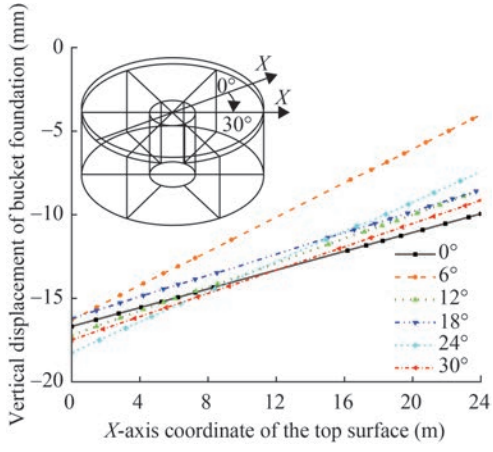

Figure 16 Vertical displacement of bucket foundation at various spudcan angles

bulkheads and the bucket bottom, extending upward to approximately halfway up the bucket wall. Furthermore, a "trapezoidal" distribution of high stress levels is observed at the bucket bottom between the bulkheads, extending upward to approximately one-third of the bucket height.

As the spudcan penetration angle deviates from 0°, the stress distribution along the bucket wall and bottom becomes increasingly uneven. In particular, a pronounced stress concentration is evident at the junction of the bulkhead and the bucket bottom on the side closer to the spudcan, forming a "trapezoidal" pattern centered around the bulkhead and extending upward to one-third of the bucket

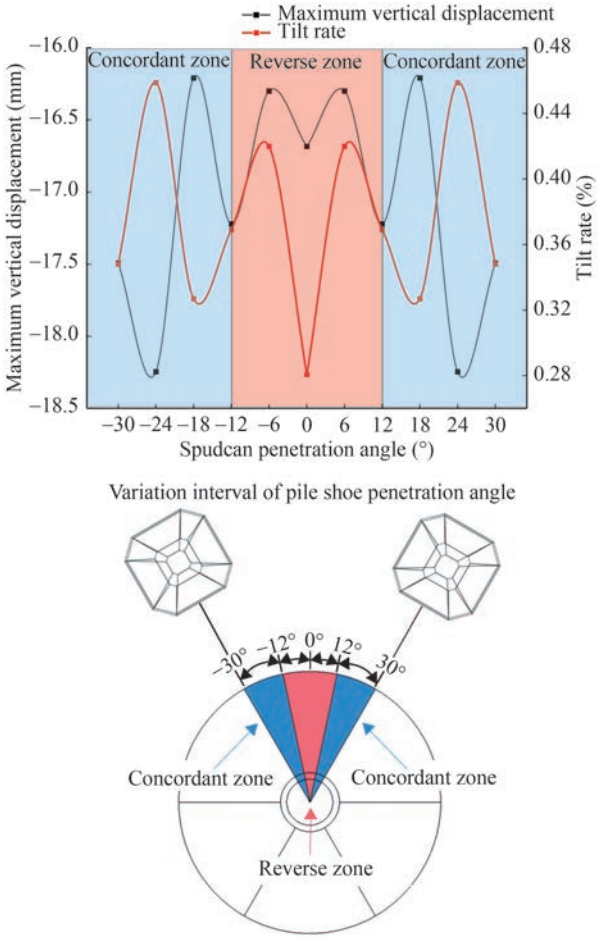

Figure 17 Vertical displacement and tilt rate of composite bucket foundation at various spudcan angles with zoning diagram

height. In contrast, the side farther from the spudcan exhibits relatively lower stress levels, with a "belt-like" distribution extending upward to approximately half of the bucket height. These findings indicate that the spudcan penetration angle significantly influences the stress distribution within the wall of the multi-compartment bucket foundation. Any deviation from the symmetric axis of a compartment (i. e., the 0° position) alters the uniformity of the bucket-soil interaction. The highest stress values are concentrated at the junction of the bulkhead and bucket bottom nearest to the spudcan.

Figures 19(a) and (b) demonstrate the stress distribution around the upper and lower perimeters of the multicompartment bucket foundation for varying spudcan penetration angles at a depth of 10 m. The stress extremes around the upper portion of the bucket exhibit a relatively uniform distribution, forming a "butterfly" pattern symmetric about the 0° axis. The spudcan penetration angle has a limited effect on the stress distribution at the upper portion of the bucket. Notably, the stress distribution around the top perimeter does not peak at the bulkhead locations. Instead, the minimum stresses are observed at the intersections of the 0° and 180° bulkheads with the bucket top, while the maximum stresses occur at the 60°, 120°, 240°, and 300° positions, which do not correspond to bulkhead intersections. A comparison of the stress distributions at the top and bottom surfaces of the bucket foundation reveals that the stress at the bottom is typically greater than that at the top, indicating that the bottom surface serves as the primary load-bearing area. Except for the 0° penetration, notable variations in stress distribution at the bucket bottom are observed for different penetration angles. However, at all penetration angles, the maximum stress consistently occurs at the 30° bulkhead position, demonstrating that the spudcan penetration angle significantly affects the stress distribution at the bucket bottom. When the spudcan penetrates at 0°, the stress distribution at the bucket bottom is symmetric about the 0° axis, with the 30° and 330° bulkhead positions exhibiting significantly higher stress levels than other positions, bearing the primary load. As the penetration angle deviates from 0°, the stress distribution at the bottom becomes asymmetrical. In particular, the stress at the 30°, 150°, and 330° bulkhead positions remains consistently higher than at other positions, with the 30° bulkhead position showing the highest stress levels. The variation in maximum contact stress with penetration angle is illustrated in Figure 20. The contact stress at the 30° and 150° bulkhead positions generally increases with penetration angle, with maximum increases of 51.92% and 83.32%, respectively. Conversely, the stress at the 330° position demonstrates a notable decrease of up to 42.22%. Figure 21 elucidates the mechanism underlying this phenomenon, demonstrating the interaction between the bucket foundation and the surrounding soil. As previously discussed, the orientation of the bucket foundation aligns with the spudcan penetration angle. The resulting relative horizontal displacement between the bucket and the soil can be decomposed into X and Y components for analyzing the primary load-bearing areas. The contact load generated by the X-direction displacement component is primarily borne by the intersections of the 30° and 150° bulkheads with the bucket bottom and their surrounding areas, which are symmetrically distributed along the 90° line. Given the pronounced soil squeezing effect caused by spudcan penetration, these areas are the primary load-bearing structures, with stress levels increasing as the net distance between the load-bearing area and the spudcan decreases. This trend is corroborated by the data presented in Figures 18 and 19(b). The Y-direction displacement component significantly influences the intersections of the 30° and 330° bulkheads with the bucket bottom and their surrounding areas. As the net distance between these areas and the spudcan increases with the penetration angle, the stress generally decreases, as shown in Figures 18 and 19(b). The 30° position consistently exhibits the highest stress levels because it bears loads from the X and Y directions.

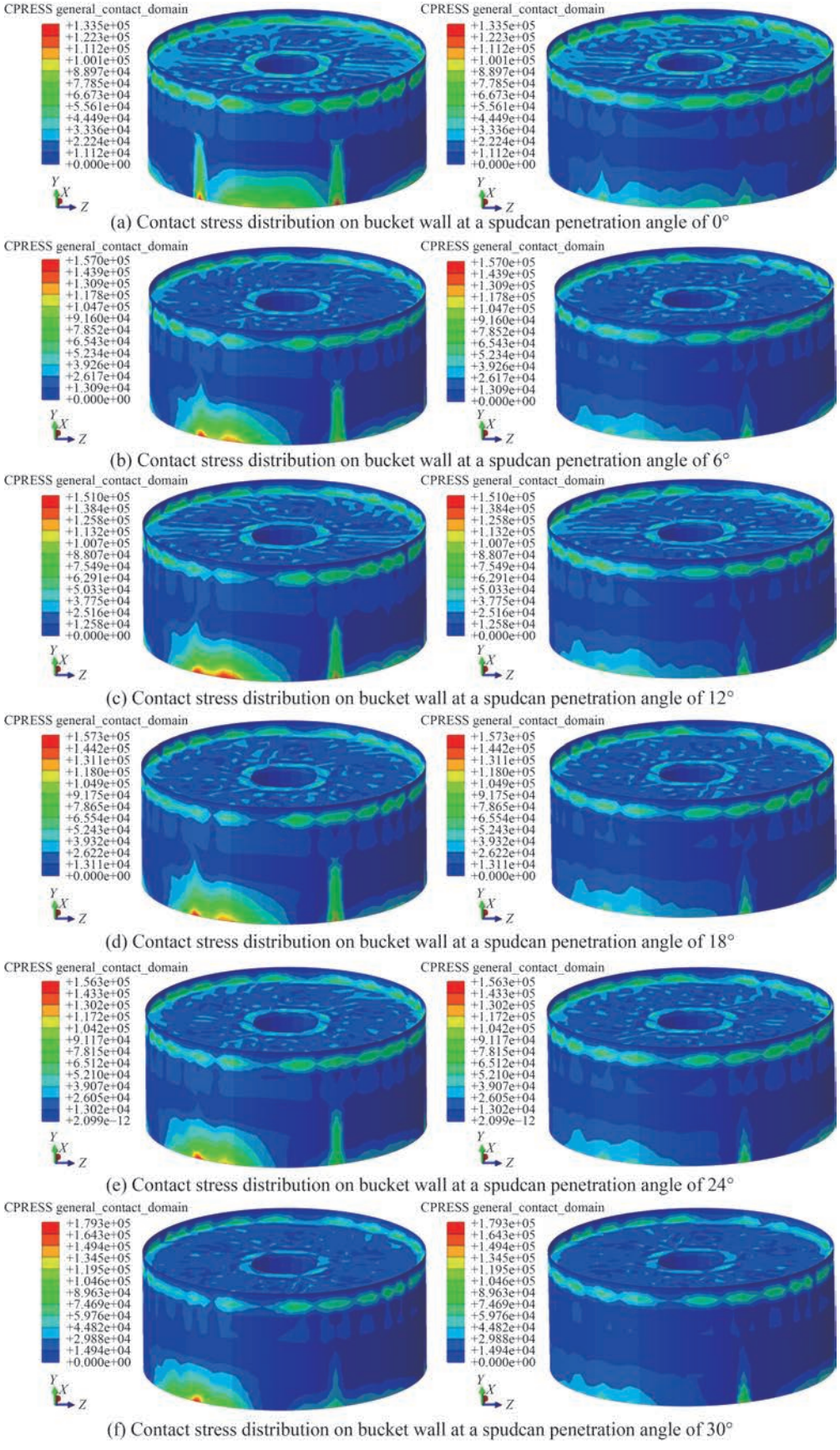

Figure 18 Stress distribution in bucket foundation at different spudcan penetration angles

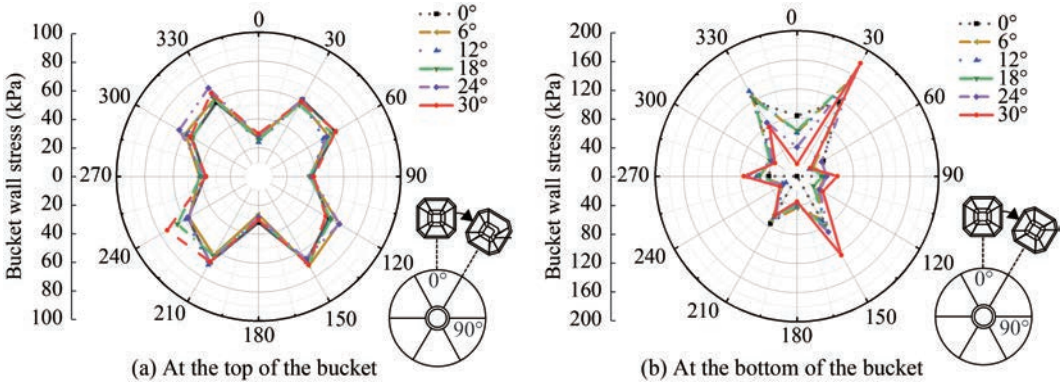

Figure 19 Distribution of contact stress

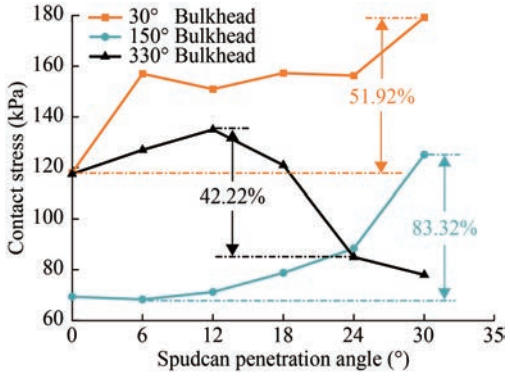

Figure 20 Maximum contact stress at the bottom of the bucket

In conclusion, the primary distribution and variation trends of contact stress induced by spudcan penetration can be determined by decomposing the relative horizontal displacement direction into orthogonal components within the horizontal plane. The load-bearing areas are the intersections of the bulkheads with the bucket bottom and their surrounding regions, which are symmetrically distributed about the displacement components and are closest to the spudcan.

Figure 22 illustrates the contact stress distribution along the embedded path at the junction of each bulkhead and the bucket wall for a multi-compartment bucket foundation, considering different spudcan penetration angles. Overall, the contact stress distribution along the paths of each bulkhead exhibits a comparable pattern. In the embedment range from 0 to 1 m (surface to 0.1*H*), a significant decline is observed in contact stress with increasing depth. This rapid reduction can be attributed to soil heave and backflow, which quickly mitigate the soil-squeezing effect, as illustrated in Figure 10. In the subsequent embedment range of 1–3 m (0.1*H* to 0.3*H*), the increase in contact stress is minimal, indicating that soil backflow diminishes and the soil remains relatively stable. In the 3–6 m (0.3*H* to the top of the spudcan) embedment range, the cumulative weight of the overlying soil and the soil-squeezing effect of the in-situ spudcan result in a renewed backflow trend. This results in a slight decrease in contact stress along the path,

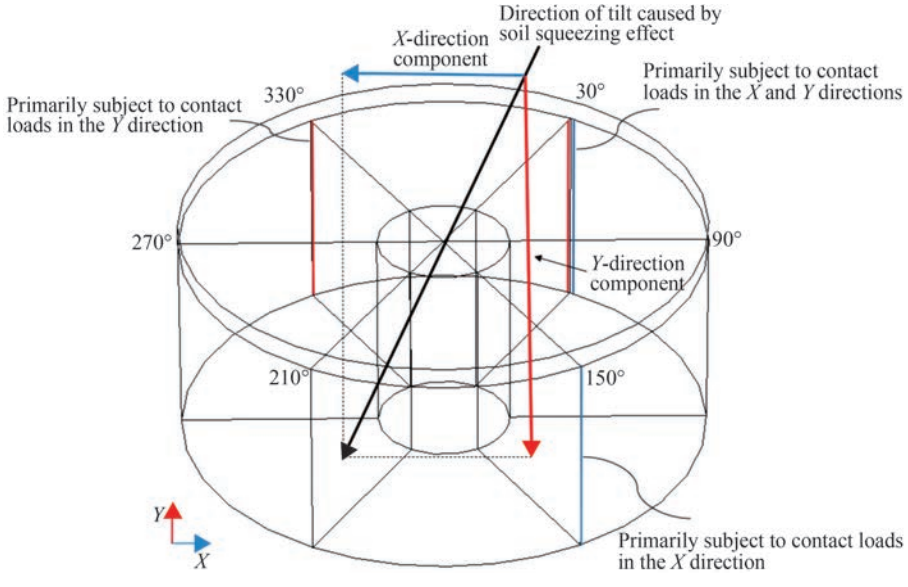

Figure 21 Mechanism of stress distribution at the bucket bottom

with the lowest stress levels occurring at this position. This point can be considered as the most fully developed instance of soil backflow. The spudcan is embedded to a depth between 6 and 10 m, so the continuous soil-squeezing effect of the in-situ spudcan restricts soil backflow near the foundation, causing a significant degree of soil compression in the lower portion of the foundation. This effect is particularly pronounced at an embedment depth of 8.8 m, where the spudcan's long edge is located. After sufficient soil compression has occurred, the contact stress along the path increases notably with depth. The upper part of the spudcan induces soil to flow back into the spudcan pit, exerting additional influence on the backflow trend within the 3–6 m embedment range. The vertical section of soil backflow under the interaction of the spudcan, multicompartment bucket foundation, and sand can be qualitatively depicted based on the spudcan penetration depth, as illustrated in Figure 23.

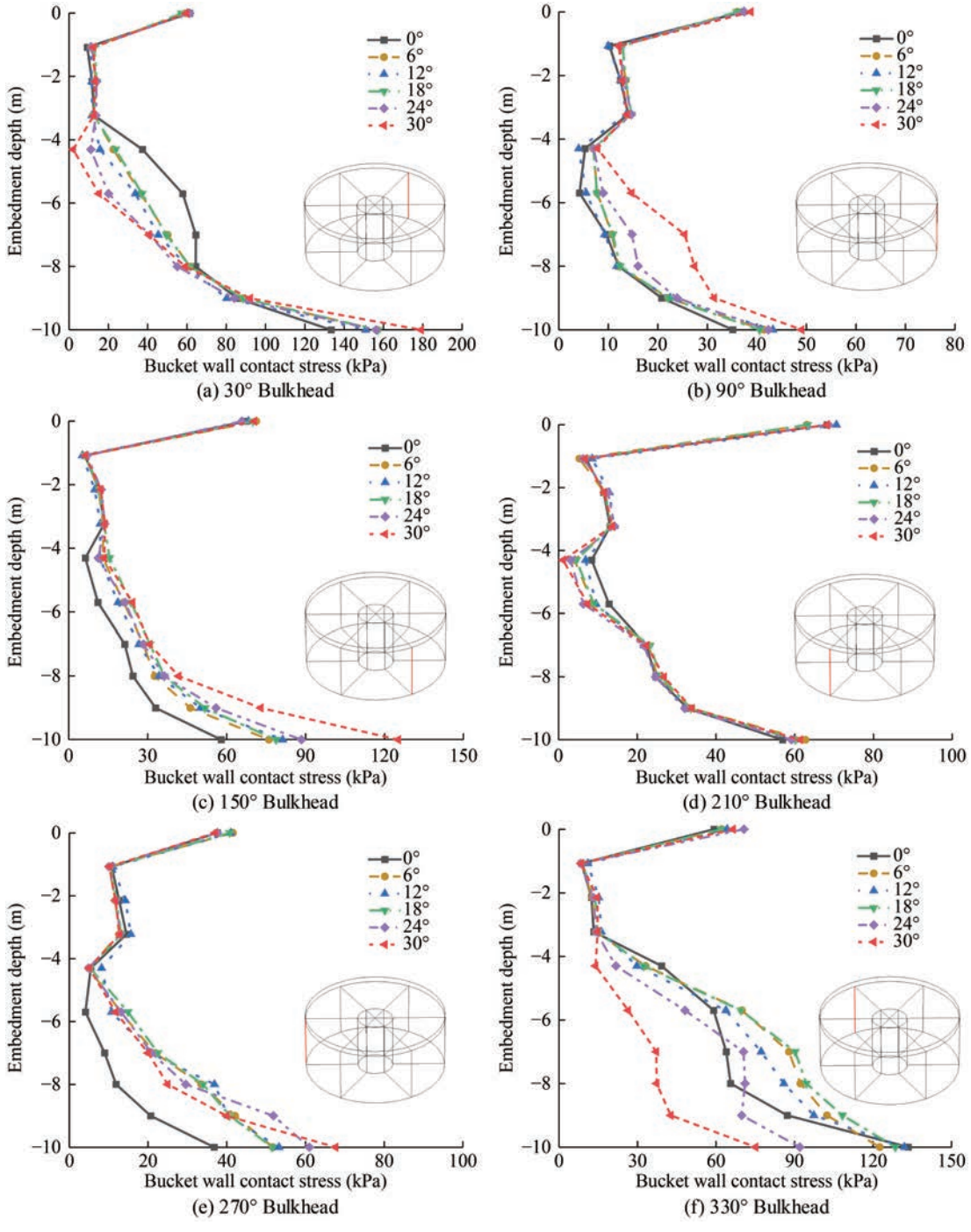

Figure 22 Contact stress distribution at the interfaces of bulkheads and bucket wall after spudcan penetration

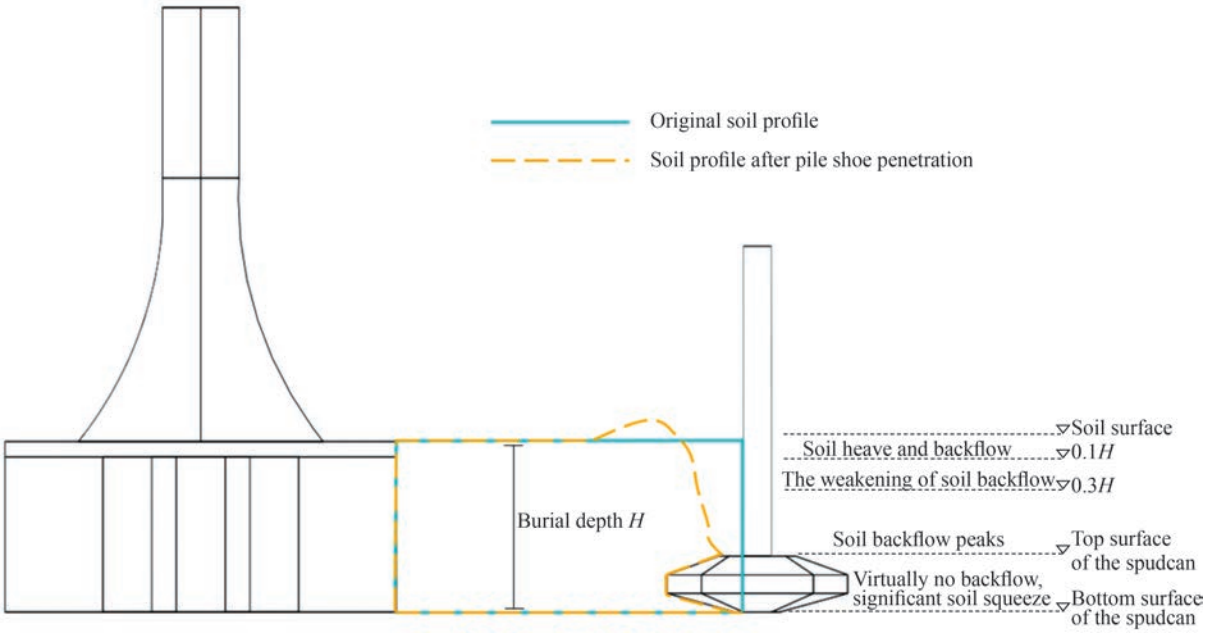

Figure 23 Soil backflow state between spudcan and composite bucket foundation in sand

4 Conclusions

This study employed physical model testing and the CEL method to investigate the effect of spudcan penetration angles on the adjacent composite bucket foundation in sand. The findings are summarized below.

1) The effect of spudcan penetration on sand is most pronounced within a distance of 1.0*d* from the spudcan's long edge. Beyond 2.0*d*, the effect diminishes substantially and becomes negligible at 2.5*d*.

2) The penetration angles of the spudcan result in soil heaving around the spudcan, with minimal backflow filling the spudcan pit. This outcome indicates limited soil backflow in dense sand. At the spudcan base, a distinct "concave" equivalent plastic strain zone is observed, where the equivalent plastic strain initially decreases and then increases as the angle increases.

3) The maximum vertical displacement and tilt rate of the multicompartment bucket foundation display a "wave-like" variation under different penetration angles. The relative trends of these two parameters are opposite for penetration angles ranging from 0° to 12° and similar for angles from 12° to 30°, delineating two distinct zones. The interval between 0° and 12° is defined as the opposite zone, and that between 12° and 30° is defined as the similar zone. The maximum vertical displacement demonstrates minimal variation across penetration angles, whereas the tilt rate varies significantly, peaking at penetration angles of 6° and 24°. Consequently, when considering the in-place stability of the multicompartment bucket foundation, particular attention should be paid to the foundation's state when the spudcan penetrates at small angles relative to the bulkhead of the bucket foundation.

4) The stress distribution on the walls of the multicompartment bucket foundation under varying penetration angles is primarily concentrated at the top and bottom of the bucket, with notable stress concentrations at the junctions of bulkheads and the sidewall. As the penetration angle deviates from the foundation's symmetry axis, the stress distribution becomes increasingly uneven, with the maximum stress shifting toward the bulkhead-bottom junction nearest to the spudcan. The formation mechanism of this phenomenon is analyzed, indicating that the stress state of the multi-compartment bucket foundation should be closely monitored when the spudcan penetrates at angles near the bulkhead.

Competing interest The authors have no competing interests to declare that are relevant to the content of this article.

Reference

Bui HH, Fukagawa R, Sako K, Ohno S (2008) Lagrangian meshfree particles method (SPH) for large deformation and failure flows of geomaterial using elastic–plastic soil constitutive model. International Journal for Numerical and Analytical Methods in Geomechanics 32(12): 1537-1570. https://doi.org/10.1002/nag.688

Chouhan K, Chavda JT (2021) A review on numerical simulation of large deformation problems in geotechnical engineering. Indian Geotechnical Conference, 167-181. https://doi.org/10.1007/978-981-19-6998-0_16

Craig WH, Chua KV (1990) Deep penetration of spud-can foundations on sand and clay. Geotechnique 40(4): 541-556. https://doi.org/10.1680/geot.1990.40.4.541

Dai XR, Wang JH, Fan YF (2018) Issues of numerical simulation of the spudcan penetration based on CEL method. Rock and Soil Mechanics 39(6): 2278-2286. DOI: 10.16285/j.rsm.2016.2142

Dao CD, Kazemtabrizi B, Crabtree CJ (2020) Offshore wind turbine reliability and operational simulation under uncertainties. Wind Energy 23(10): 1919-1938. https://doi.org/10.1002/we.2526

Ding H, Feng Z, Zhang P, Le C, Guo Y (2020) Floating performance of a composite bucket foundation with an offshore wind tower during transportation. Energies 13(4): 882. https://doi.org/10.3390/en13040882

Ding H, Zhao X, Le C, Zhang P, Min Q (2019) Towing motion characteristics of composite bucket foundation for offshore wind turbines. Energies 12(19): 3767. https://doi.org/10.3390/en12193767

Domingos DF, Atzampou P, Meijers PC, Beirão SH, Metrikine AV, van Wingerden JW, Wellens P (2024) Full-scale measurements and analysis of the floating installation of an offshore wind turbine tower. Ocean Engineering 310: 118670. https://doi.org/10.1016/j.oceaneng.2024.118670

Falcon SS, Choo YW, Leung CF (2021) Pile behavior due to adjacent jack-up spudcan penetration. International Journal of Offshore and Polar Engineering 31(4): 472-479. https://doi.org/10.17736/ijope.2021.jc823

Fan Y, Wang J (2021) Method to evaluate effect of spudcan penetration on adjacent jacket piles. Applied Ocean Research 106: 102436. https://doi.org/10.1016/j.apor.2020.102436

Hossain M, Randolph M (2010) Deep-penetrating spudcan foundations on layered clays: centrifuge tests. Geotechnique 60(3): 157-170. https://doi.org/10.1680/geot.8.P.039

Le CH, Hu H, Wang X, Ren JY, Zhang PY, Ding HY (2024) study on influence of spudcan penetration pile on adjacent bucket foundation in sandy soil. Acta Energiae Solaris Sinica 45(2): 95-101. DOI: 10.19912/j.0254-0096.tynxb.2022-1624

Li S, Wang Z, Jia X, He L (2018) Response study of jacket piles induced by spudcan penetration. ASME 2018 37th International Conference on Ocean, Offshore and Arctic Engineering, V009T10A032. https://doi.org/10.1115/OMAE2018-78337

Liu R, Cao TM, Chen GS, Zhang HY, Li CF (2020) Experimental study of the effect of spudcan penetration and extraction on bearing capacity of an adjacent spudcan. Rock and Soil Mechanics 41(9): 2943-2952. DOI: 10.16285/j.rsm.2019.1905

Ma X, Li M, Li W, Liu Y (2025) Overview of offshore wind power technologies. Sustainability 17(2): 596. https://doi.org/10.3390/su17020596

Qiu G, Henke S (2011) Controlled installation of spudcan foundations on loose sand overlying weak clay. Marine Structures 24(4): 528-550. https://doi.org/10.1016/j.marstruc.2011.06.005

Qiu G, Henke S, Grabe J (2011) Application of a coupled Eulerian–Lagrangian approach on geomechanical problems involving large deformations. Computers and Geotechnics 38(1): 30-39. https://doi.org/10.1016/j.compgeo.2010.09.002

Shi J, Hu M, Zhang Y, Chen X, Yang S, Hallak TS, Chen M (2024) Dynamic analysis of crane vessel and floating wind turbine during temporary berthing for offshore on-site maintenance operations. Journal of Marine Science and Engineering 12(8): 1393. https://doi.org/10.3390/jmse12081393

Siciliano RJ, Hamilton JM, Murff J, Phillips RJ (1990) Effect of jackup spud cans on piles. Offshore Technology Conference, Houston, OTC-6467-MS. https://doi.org/10.4043/6467-MS

Teh KL, Cassidy MJ, Leung CF, Chow YK, Randolph MF, Quah CK (2008) Revealing the bearing capacity mechanisms of a penetrating spudcan through sand overlying clay. Géotechnique 58(10): 793-804. https://doi.org/10.1680/geot.2008.58.10.793

Tho KK, Leung CF, Chow YK, Swaddiwudhipong S (2013) Eulerian finite element simulation of spudcan–pile interaction. Canadian Geotechnical Journal 50(6): 595-608. https://doi.org/10.1139/cgj-2012-0288

Tian Y, Cassidy MJ, Randolph MF, Wang D, Gaudin C (2014) A simple implementation of RITSS and its application in large deformation analysis. Computers and Geotechnics 56: 160-167. https://doi.org/10.1016/j.compgeo.2013.12.001

Wang D, Bienen B, Nazem M, Tian Y, Zheng J, Pucker T, Randolph MF (2015) Large deformation finite element analyses in geotechnical engineering. Computers and Geotechnics 65: 104-114. https://doi.org/10.1016/j.compgeo.2014.12.005

Wu Q, Liu R, Zhang H, Wang Y (2018) Bucket spudcan penetration resistance in saturated sand. China Earthquake Engineering Journal 40(6): 183-1190

Xie Y (2009) Centrifuge model study on Spudcan-pile interaction. PhD thesis, National University of Singapore, 93-97

Xie Y, Leung CF, Chow YK (2012) Centrifuge modelling of spudcan–pile interaction in soft clay. Géotechnique 62(9): 799-810. https://doi.org/10.1680/geot.12.OG.003

Xie Y, Leung CF, Chow YK (2017) Centrifuge modelling of spudcan–pile interaction in soft clay overlying sand. Géotechnique 67(1): 69-77. https://doi.org/10.1680/jgeot.15.P.031

Zhang JH, Yan J, Wu WJ, Liu YQ (2019) Research on short-term forecasting and uncertainty of wind turbine power based on relevance vector machine. Energy Procedia 158: 229-236. https://doi.org/10.1016/j.egypro.2019.01.081

Zhang P, Ding H, Le C, Huang X (2013) Motion analysis on integrated transportation technique for offshore wind turbines. Journal of Renewable and Sustainable Energy 5: 053117. https://doi.org/10.1063/1.4822056

Zhang P, Li J, Gan Y, Zhang J, Qi X, Le C, Ding H (2020) Bearing capacity and load transfer of brace topological in offshore wind turbine jacket structure. Ocean Engineering 199: 107037. https://doi.org/10.1016/j.oceaneng.2020.107037

Zhang P, Qi X, Ding H, Le C, Lin Y, Xiao J (2023) Bearing characteristics of mono-column composite bucket foundation in sand for offshore wind turbines. Ocean Engineering 280: 114870. https://doi.org/10.1016/j.oceaneng.2023.114870

Zhou ZJ, Qi CG, Kong GQ, Zhong FT, Zhang ZC, Lai WJ (2023) Research on mechanism of jack-up drilling platform spudcan penetrating into saturated sand. Engineering Mechanics 40(6): 144-157. DOI: 10.6052/j.issn.1000-4750.2021.11.0891